Crystal-field analysis of the energy levels and spectroscopic characteristics of Nd^{3+} in $YAl_3(BO_3)_4$ crystal

1998 J. Phys.: Condens. Matter 10 5147

(http://iopscience.iop.org/0953-8984/10/23/015)

J. Phys.: Condens. Matter **10** (1998) 5147–5160. Printed in the UK PII: S0953-8984(98)90012-1

Crystal-field analysis of the energy levels and spectroscopic characteristics of Nd^{3+} in $YAl_3(BO_3)_4$ crystal

Chen Xueyuan† and Luo Zundu†‡

† Fujian Institute of Research on the Structure of Matter, Chinese Academy of Sciences, Fuzhou, Fujian 350002, People's Republic of China

‡ China Centre of Advance Science and Technology (World Laboratory), PO Box 8730, Beijing 100080, People's Republic of China

Received 10 December 1997, in final form 19 March 1998

Abstract. On the basis of the analysis of the group-chain scheme ($SO_3 \supset O \supset D_3$), the crystal-field-level fitting has been carried out for Nd^{3+}:$YAl_3(BO_3)_4$, in which the Nd^{3+} ions occupy D_3 site symmetry positions. The RMS value of the energy-level fitting is 8.95 cm^{-1} and the group character of each Stark level compares well to the experimental assignment on the whole. The wavefunctions obtained were used in the study of the Zeeman interaction and the fluorescence spectra. The calculated *g*-factors obey Karayianis's partial *g*-sum rule, and the *g*-factor of the ground state of $^4I_{9/2}$ is predicted. According to the Judd–Ofelt theory, the odd crystal-field parameters have been quantitatively determined by the fit to the experimental transition rates from $^4F_{3/2}$. The line-to-line transition rates and thus the fluorescence spectra from $^4F_{3/2}$ at room temperature have been calculated, which are in agreement with the experiment by and large.

1. Introduction

Neodymium doped yttrium aluminum borate, Nd^{3+}:$YAl_3(BO_3)_4$, hereafter referred to as NYAB, has been demonstrated to be an ideal self-frequency-doubling (SFD) laser crystal with a rather high nonlinear optical coefficient and a large stimulated emission cross section up to 10.0×10^{-19} cm^2 at 1062 nm [1]. At the same time, it has excellent chemical and physical properties important for a laser device, such as high hardness comparable to that of the YAG crystal, anti-deliquescence and absence of colour centres etc. Therefore the NYAB crystal has bright prospects of wide practical applications. Small and compact laser-diode (LD) pumping solid state lasers emitting green light have been realized, which is useful in the fields of medical surgery, communications and computer technology. In fact, this laser system has been operated under a variety of schemes [1–7] and continuous-wave (CW) green powers up to 50 mW have been reached [6]. Very recently, Jaque [2] has done a complete spectroscopic work on this material. Most of the energy levels of Nd^{3+} have been identified for the first time, which provides a full characterization of the spectroscopy of NYAB. In addition, infrared to visible upconversion fluorescence and CW laser properties in this crystal have been reported [8].

It is important to study the detailed energy-level structures of laser crystals in order to improve the laser efficiency. The crystal-field analysis using the group-chain scheme has been proved very useful and effective in the study of the spectroscopic properties of localized centres in the crystals [9–13]. Although one of us performed the group-chain scheme analysis of this crystal [9], the result of the energy-level fitting was not satisfying and the

0953-8984/98/235147+14$19.50

root mean square (RMS) deviation (about 20 cm^{-1}) is somewhat large. The experimental energy levels adopted at that time were done by Amano and Mochizuki [4]. There are some discrepancies between Amano's and Jaque's data [2]. Energy levels identified by Jaque, we believe, are more accurate and reasonable in that the fluorescence and absorption spectra were recorded at low temperature (10 K) and the resolution was of great accuracy (<3 cm^{-1}). As shown in the following, the present fitting results will also confirm this point.

Thanks to Jaque's careful identifying the position and group character of the Stark levels by their experiment, we are able to theoretically perform the energy-level fitting with great confidence. In this paper, group-chain scheme analysis as previously proposed will be applied to Nd^{3+} ions occupying the D_3 symmetry site of the NYAB crystal. Taking advantage of the fitting wavefunctions, we can further calculate the paramagnetic splitting g-tensors and the line-to-line fluorescence intensities between Stark sublevels. The results will be compared with the experiment.

2. Group-chain scheme analysis

The site symmetry of Nd^{3+} ions in $YAl_3(BO_3)_4$ is D_3. In the case of the D_3 group, Butler's notations [14] $0, \tilde{0}, 1, \frac{1}{2}, \frac{3}{2}$ and $-\frac{3}{2}$ correspond to Γ_1, Γ_2, Γ_3, Γ_4, Γ_5 and Γ_6 respectively, of Bethe's notation. In NYAB, the Nd^{3+} ion contains 3 4f-shell electrons and is an odd-electron system. So its CF Hamiltonian is a time-reversal invariant, which leads to Kramers degeneracy of all Stark levels. Consider the group chain $SO_3 \supset O \supset D_3$; the detailed CF Hamiltonian can be expressed in Butler's notation

$$H_{cf} = \sum_{k\mu} C_\mu^k b_\mu^k = C_{\tilde{1}}^2 b_{\tilde{1}}^2 + C_{\tilde{1}}^3 b_{\tilde{1}}^3 + C_0^4 b_0^4 + C_{\tilde{1}}^4 b_{\tilde{1}}^4 + C_{\tilde{1}}^5 b_{\tilde{1}}^5 + C_0^6 b_0^6 + C_{\tilde{1}_0}^6 b_{\tilde{1}_0}^6 + C_{\tilde{1}_1}^6 b_{\tilde{1}_1}^6. \quad (1)$$

Here b_μ^k are the basis functions of the group chain $SO_3 \supset O \supset D_3$ and are associated with $|k\mu 0\rangle$ in [14]; C_μ^k are the expansion coefficients of H_{cf} by these bases. Because all the basis functions belong to the 0 representation of D_3, the index 0 for D_3 group has been omitted. The k-even CF components result in the experimentally observed Stark splitting of rare-earth spectra, whereas the k-odd CF components, via configuration admixture, bring about the electric dipole (ED) transition within the $4f^n$ configuration according to Judd–Ofelt (JO) theory [15, 16]. In (1), the effect of the $4f^{n-1}5g^1$ configuration or seventh-order odd CF components ($C_{\tilde{1}_0}^7 b_{\tilde{1}_0}^7$ and $C_{\tilde{1}_1}^7 b_{\tilde{1}_1}^7$) is neglected for the reasons explained in [10].

The Hamiltonian can also be expanded as follows by the conventional CF scheme:

$$\begin{aligned} H_{cf} &= \sum_{kq} B_{kq} C_{kq} \\ &= B_{20}C_{20} + B_{33}(C_{33} + C_{3-3})B_{40}C_{40} + B_{43}(C_{43} + C_{4-3}) \\ &\quad + B_{53}(C_{53} + C_{5-3})B_{60}C_{60} + B_{63}(C_{63} + C_{6-3}) + B_{66}(C_{66} + C_{6-6}) \end{aligned} \quad (2)$$

where B_{43} and B_{63} have been made real by a 90° rotation about the crystal Z axis, while B_{33} and B_{53} have been made imaginary. In other words, one of three twofold rotations is aligned along the Y axis, rather than along the X axis, which is different from the axis choice in Sachs's book [17].

It can be easily proved that the relationship between the CF parameters of these two different schemes will be

$$\begin{aligned}
B_{20} &= -C^2_{\tilde{1}} \\
B_{33} &= -\frac{1}{\sqrt{2}}C^3_{\tilde{1}} \\
B_{40} &= (-\tfrac{1}{3})(\tfrac{7}{3})^{1/2}C^4_0 - (\tfrac{2}{3})(\tfrac{5}{3})^{1/2}C^4_{\tilde{1}} \\
B_{43} &= (-\tfrac{1}{3})(\tfrac{10}{3})^{1/2}C^4_0 + (\tfrac{1}{3})(\tfrac{7}{6})^{1/2}C^4_{\tilde{1}} \\
B_{53} &= \frac{1}{\sqrt{2}}C^5_{\tilde{1}} \\
B_{60} &= (-\tfrac{4}{9})(2)^{1/2}C^6_0 + (\tfrac{7}{9})C^6_{\tilde{1}_1} \\
B_{63} &= (\tfrac{1}{9})(\tfrac{35}{3})^{1/2}C^6_0 + (\tfrac{11}{42})^{1/2}C^6_{\tilde{1}_0} + (\tfrac{4}{9})(\tfrac{10}{21})^{1/2}C^6_{\tilde{1}_1} \\
B_{66} &= (-\tfrac{1}{9})(\tfrac{77}{6})^{1/2}C^6_0 + (\tfrac{5}{21})^{1/2}C^6_{\tilde{1}_1} - (\tfrac{4}{9})(\tfrac{11}{21})^{1/2}C^6_{\tilde{1}_1}.
\end{aligned} \tag{3}$$

Note that there are a few mistakes in the conversion expression given in (7) in [9], and it should be corrected as (3).

The wavefunctions of all Stark levels can be expressed as

$$\Psi = \sum_{aa_1a_2} C^a_{a_1a_2}|aa_1a_2\rangle. \tag{4}$$

The matrix elements of the CF Hamiltonian can be calculated by means of the Wigner–Eckart theorem and the factorization lemma of the $3jm$ factors.

$$\begin{aligned}
\langle aa_1a_2|H_{cf}|bb_1b_2\rangle = &\sum_{k\mu} C^k_\mu \begin{pmatrix} a \\ a_1 \end{pmatrix} \begin{matrix} \mathrm{SO_3} \\ \mathrm{O} \end{matrix} \begin{pmatrix} a_1 \\ a_2 \end{pmatrix} \begin{matrix} \mathrm{O} \\ \mathrm{D_3} \end{matrix} \\
&\times \sum_{rr_1r_2} \begin{pmatrix} a^* & k & b \\ a_1^* & \mu & b_1 \end{pmatrix} \begin{matrix} r & \mathrm{SO_3} \\ r_1 & \mathrm{O} \end{matrix} \begin{pmatrix} a_1^* & \mu & b_1 \\ a_2^* & 0 & b_2 \end{pmatrix} \begin{matrix} r_1 & \mathrm{O} \\ r_2 & \mathrm{D_3} \end{matrix} \langle a\|b^k\|b\rangle
\end{aligned} \tag{5}$$

$$\langle a\|b^k\|b\rangle = \langle \mathrm{f}^n SLa\|U^{(k)}\|\mathrm{f}^n S'L'b\rangle\langle 4\mathrm{f}\|C^{(k)}\|4\mathrm{f}\rangle. \tag{6}$$

The reduced matrix elements (RMEs) $\langle \mathrm{f}^n SLa\|U^{(k)}\|\mathrm{f}^n S'L'b\rangle$ can be calculated by using the intermediate-coupling wavefunction provided by Wybourne [18]. All the $2jm$ and $3jm$ factors for the group chain $\mathrm{SO_3} \supset \mathrm{O} \supset \mathrm{D_3}$ can be found from [14]. The energy-level fitting is performed by two steps instead of by diagonalizing a combined spin–orbit and CF Hamiltonian. First, free-ion wavefunctions in a Russell–Saunders basis of J-states are obtained by diagonalizing a Hamiltonian containing the Coulomb and spin–orbit interactions, and thus we can compute the RME of $U^{(k)}$ ($k = 2, 4, 6$) between all of the intermediate-coupled wavefunctions. Second, matrices representing the even CF interaction are diagonalized simultaneously for $^{2S+1}L_J$ states (including $^4\mathrm{I}_{9/2}$, $^4\mathrm{I}_{11/2}$, $^4\mathrm{I}_{13/2}$ and $^4\mathrm{F}_{3/2}$), and the even CF parameters are determined by a least-squares fit to the experimental energy levels. Here we assume that the centres of the gravity of J-multiplets are invariant even in the CF interaction, neglecting the effect of J-mixing in NYAB.

On the basis of the group–subgroup chain $\mathrm{SO_3} \supset \mathrm{O} \supset \mathrm{D_3}$, the wavefunctions of the $4f^3$ configuration in Nd^{3+} at the D_3 symmetry position are expressed as linear combinations of the bases $|\mathrm{f}^n SLJ\mu\nu\rangle$, where μ and ν are the irreducible representations of O and D_3 respectively. The detailed matrix elements of all the terms can be obtained from (5). The conventional CF parameters are calculated by the simple point-charge model. Consider

the shielding factors of $5s^2 5p^6$ shells and the scaling parameters of the bare Hartree–Fock wavefunction [19],

$$B_{kq} = \rho_k A_{kq}. \tag{7}$$

With Nd^{3+}:

$$\rho_2 = 0.1706 \qquad \rho_4 = 0.5776 \qquad \rho_6 = 1.5897.$$

A_{kq} is the result of the lattice sum. Hence the initial values of CF parameters (B_{kq} and C_μ^k) can be obtained by using the crystal structure of NYAB [9], and are listed in tables 1 and 2.

Table 1. CF parameters B_{kq} for NYAB (in cm^{-1}).

B_{20}	B_{40}	B_{43}	B_{60}	B_{63}	B_{66}	Reference
125	−4685	−2387	1308	−377	−528	point-charge model
−186	624	356	−210	74	86	[9]
342	207	1373	50	−260	94	fitting results

Table 2. Group-chain parameters C_μ^k for NYAB (in cm^{-1}).

$C_{\bar{1}}^2$	C_0^4	$C_{\bar{1}}^4$	C_0^6	$C_{\bar{1}_0}^6$	$C_{\bar{1}_1}^6$	Reference
−125	5291	2314	−688	−901	1125	point-charge model
228	−1569	−587	456	605	−658	[9]
−342	−1776	810	−303	−175	−181	fitting results

The final k-even parameters C_μ^k and the corresponding B_{kq} can be obtained by adjusting the initial values to minimize the RMS deviation of the energy levels in the least-squares fit, which are also given in tables 1 and 2. A comparison of the experimental and fitting energy levels, as well as the group attributes of Stark sublevels, are shown in table 3. The wavefunctions of all Stark levels are normalized and listed in order of increasing energy in the appendix. There are 20 levels with the greatest experimental confidence in this fit, giving a final RMS of 8.95 cm^{-1}.

Tables 1 and 2 show that there are significant difference between this work and [9] although both were fitted by using the group-chain scheme. One can see that CF parameters (B_{kq} and C_μ^k) change values or signs. The major reason for the difference may be due to the different choices of the experimental levels as mentioned in section 1. For a better understanding of this point we can compare the experimental levels between two sources (Jaque's [2] and Amano's [4] data). For example, the Stark levels of the ground state $^4I_{9/2}$ term from [2] locate at 0, 48, 109, 165 and 289 cm^{-1}, while those from [4] lie at 0, 105, 158, 324 and 324 cm^{-1}. There exist great discrepancies between them. Furthermore, as is well known, many minima exist in the nonlinear least-squares fit to the experimental levels, and all of them may have a small RMS deviation but they do not all correspond to physical reality. This results in the variable parameters determined by the fit often being sensitive to the values of experimental levels to be fitted. Hence it is not difficult to understand that the CF parameters determined in this work differ greatly from those of [9]. Comparing with the results of [9] (RMS = 20.2 cm^{-1}, at 77 K), we can see that the calculated eigenvalues agree better with the experimental energy levels, which indicates that the present set of CF parameters is more reliable than before.

In this paper only 20 levels of $^4I_{9/2}$, $^4I_{11/2}$, $^4I_{13/2}$ and $^4F_{3/2}$ multiplets are included and fitted in the group-chain scheme. No doubt the energy-level fitting should involves more multiplets in order to estimate the reliability of the CF parameters. However, the effect of J-mixing and the interaction with excited configurations should not be ignored in the calculation as far as the high-lying multiplets are concerned, since the energy levels of those terms are more closely spaced and adjacent to excited configurations. Then the energy-level fitting should be performed by full diagonalization of a combined free-ion and CF Hamiltonian instead of by the two-step method proposed in this paper, which can be discussed in our later work. Were the effect of J-mixing and other interactions not taken into account, the RMS deviation would often increase when more multiplets are involved in the present fit.

Table 3. Comparison of the observed and calculated energy levels and g-factors of NYAB at 10 K.

	Energy (cm^{-1})				g-factor	
J-multiplet	Γ (exp.)[a]	Experimental[a]	Γ (calc.)	Calculated	$g_\parallel$	$g_\perp$
$^4I_{9/2}$	4	0	4	−8	**1.332**	3.552
	5,6	48	5,6	41	5.428	0
	5,6	109	4	116	**−0.200**	2.832
	4	165	5,6	167	3.191	0
	4	289	4	296	**1.047**	3.247
$^4I_{11/2}$	4	1945	4	1957	**−4.139**	3.189
	4	1968	5,6	1973	6.232	0
	—	1982	4	1988	**−1.753**	0.665
	4	2082	4	2074	**−3.260**	3.311
	—	2127	5,6	2125	5.338	0
	4	2165	4	2151	**1.432**	5.248
$^4I_{13/2}$	4	3900	4	3895	**2.145**	6.246
	4	3912	5,6	3916	6.843	0
	5,6	3931	4	3923	**0.852**	4.739
	4	3952	4	3965	**6.064**	3.048
	4	4068	4	4057	**−4.405**	3.837
	5,6	4097	5,6	4099	6.425	0
	4	4114	4	4120	**0.885**	7.018
$^4F_{3/2}$	4	11 391	4	11 390	**0.397**	0.795
	5,6	11 440	5,6	11 441	1.192	0

[a] [2]; — denotes the group character of this level cannot be determined.

As shown in table 3, not only the calculated CF levels but also the group attributes (irreducible representations) of the levels are in good agreement with those of Jaque's experiment [2] except for three pairs of the Stark levels of $^4I_{9/2}$, $^4I_{11/2}$ and $^4I_{13/2}$ manifolds. Furthermore, the group attributes of some CF levels which cannot be determined by the experiment have been theoretically identified. Note that the CF quantum number $\mu = \frac{1}{2}, \frac{3}{2}$ and $-\frac{3}{2}$ of Nd^{3+} ions in the D_3 symmetry site adopted by Jaque [2] correspond to Γ_4, Γ_5 and Γ_6 representations respectively. Let us focus on the group attribute of the ground level of $^4F_{3/2}$ manifolds. It is Γ_4 by our present fit, in accordance with Jaque's experiment and in contradiction to $\Gamma_{5,6}$ identified by Amano [4], which indicates that Amano's assignment maybe is a mistake.

3. The Zeeman interaction

Owing to Kramers degeneracy, all the Stark sublevels are doubly degenerate even if they are completely split by the CF interaction. Degenerate levels will be split in a magnetic field, and the magnitude of the splitting which can be characterized by a g-tensor depends on the external magnetic field and the wavefunctions of the CF levels. Previously we have reported the theoretical calculation of the g-tensor of the ground and excited states on the basis of the group-chain scheme analysis [11]. The detailed derivation of the formula of the g-factor is also presented there. Similarly by using the wavefunctions listed in the appendix and the formulas in [11], $g_\parallel$- and $g_\perp$-values of the Stark levels corresponding to the g-factors when the magnetic field H is along or perpendicular to the crystal Z axis respectively, are calculated and listed in table 3. For the first time, all the $g_\parallel$- and $g_\perp$-value of the ground and excited states are given. The $g_\parallel$- and $g_\perp$-value of the lowest level of the ground state $^4I_{9/2}$ are 1.332 and 3.552 respectively. Due to the lack of the experimental g-factors, we cannot compare and appraise present results in table 3. However we believe the future measurements of g-factors for NYAB will support these results. In order to confirm the reliability of the proposed method, we may sum all the g-factors over levels belonging to the Γ_4 irreducible representation of a particular $^{2S+1}L_J$ state to check the partial g-sums rule of Karayianis [20] (these $g_\parallel$ values are given in boldface in table 3). The sums are compared with theoretical values in table 4. It shows that present results are in complete agreement with the partial g-sums rule. As for the Stark levels belonging to $\Gamma_{5,6}$, one cannot define a sign for $g_\parallel$ and thus cannot perform the partial g-sums because two subspaces belonging to Γ_5 and Γ_6 irreducible representations are connected by the Zeeman Hamiltonian.

Table 4. Comparison of partial g-sums with theoretical values for the terms of NYAB. μ is the crystal quantum number.

	Γ_4 (or 1/2) of D_3	
J	$\mu = 1/2$[a]	NYAB[b]
$^4I_{9/2}$	2.18	2.179
$^4I_{11/2}$	−7.72	−7.720
$^4I_{13/2}$	5.54	5.541
$^4F_{3/2}$	0.40	0.397

[a] Theoretical values [20].
[b] Present results.

4. Study of the line-to-line fluorescence emissions from $^4F_{3/2}$

As mentioned in (1) of section 2, k-odd CF parameters play a key role in the ED transitions within $4f^n$ configurations. The effect of the $4f^{n-1}5g^1$ configuration is neglected. Therefore we can concentrate only on the excited configuration of $4f^25d^1$ and consider only the interactions of components $C_{\tilde{1}}^3 b_{\tilde{1}}^3$ and $C_{\tilde{1}}^5 b_{\tilde{1}}^5$. According to the group-chain $SO_3 \supset O \supset D_3 \supset C_3$ in NYAB, the ED moment operators are given by

$$P_{\xi\beta} = -e \sum_i (b^1_{1\xi\beta})_i r_i \tag{8}$$

where 1, 1, ξ and β are irreducible representations of the group-chain $SO_3 \supset O \supset D_3 \supset C_3$; β is the projection of ξ representation; $P_{\xi\beta}$ has three components: $\xi\beta = \tilde{0}0$ and 1 ± 1

corresponding to one π and two σ polarization spectra respectively. Table 5 lists the polarization and the selection rules for ED transitions in the case of D_3 symmetry.

Table 5. Selection rules for induced ED transitions for Nd^{3+} ions in D_3 symmetry.

	Γ_4	Γ_5	Γ_6
Γ_4	σ, π	σ	σ
Γ_5	σ	—	π
Γ_6	σ	π	—

Based on the wavefunctions obtained, we can calculate the line-to-line transition rates quantitatively for the emissions from $^4F_{3/2}$. The calculation is nearly the same as that of Nd^{3+}:YVO_4 [10] except that the line-to-line transition rates (or emission cross sections) instead of the relative intensities are calculated. For states $\langle f^n SLJa_1a_2\alpha|$ and $|f^n S'L'J'd_1d_2\gamma\rangle$, where J, a_1, a_2, α and J', d_1, d_2, γ correspond to the irreducible representations of $SO_3 \supset O \supset D_3 \supset C_3$. The transition matrix element between initial and final states can be derived as

$$\begin{aligned}\langle f^n SLJa_1a_2\alpha|P_{\xi\beta}|f^n S'L'J'd_1d_2\gamma\rangle = &-\frac{2e\langle nl|r|n'l'\rangle\langle nl\|C^{(1)}\|n'l'\rangle}{\Delta(5d)}\sum_{kk_1} C^k_{k_1} \\ &\times \sum_{\lambda e_1 e_2 S S_1 S_2} (-1)^{k-1}(2\lambda+1)\begin{pmatrix}\lambda & SO_3 & e_1\\ e_1 & O & e_2\end{pmatrix}\begin{pmatrix}e_2 & O & D_3\\ \mu & D_3 & C_3\end{pmatrix} \\ &\times \begin{pmatrix}1 & k & \lambda^*\\ 1 & k_1 & e_1^*\end{pmatrix}\begin{matrix}SO_3 & s\\ O & s_1\end{matrix}\begin{pmatrix}1 & k_1 & e_1^*\\ \xi & 0 & e_2^*\end{pmatrix}\begin{matrix}O & s_1\\ D_3 & s_2\end{matrix}\begin{pmatrix}\xi & 0 & e_2^*\\ \beta & 0 & \mu^*\end{pmatrix}\begin{matrix}D_3 & s_2\\ C_3 & \end{matrix} \\ &\times\langle n'l'\|C^{(k)}\|nl\rangle\begin{Bmatrix}1 & k & \lambda\\ l & l & l'\end{Bmatrix}\begin{pmatrix}J & SO_3 & a_1\\ a_1 & O & a_2\end{pmatrix}\begin{pmatrix}a_2 & O & D_3\\ \alpha & D_3 & C_3\end{pmatrix} \\ &\times\sum_{rr_1r_2}\begin{pmatrix}J^* & \lambda & J'\\ a_1^* & e_1 & d_1\end{pmatrix}\begin{matrix}SO_3 & r\\ O & r_1\end{matrix}\begin{pmatrix}a_1^* & e_1 & d_1\\ a_2^* & e_2 & d_2\end{pmatrix}\begin{matrix}O & r_1\\ D_3 & r_2\end{matrix} \\ &\times\begin{pmatrix}a_2^* & e_3 & d_3\\ \alpha^* & \mu & \gamma\end{pmatrix}\begin{matrix}D_3 & r_2\\ C_3 & \end{matrix}\langle f^n SLJ\|U^{(\lambda)}\|f^n S'L'J'\rangle \end{aligned} \tag{9}$$

where $k = 3, 5$; $\Delta(5d)$ is the energy separation between the initial (or final) states and the intermediate states belonging to the $4f^25d^1$ configuration with different parity. For Nd^{3+}, $\Delta(5d) = 5800\ cm^{-1}$, $\langle 4f|r|5d\rangle = 0.869$ (atomic units) [15]. All other symbols have the same physical meanings as in [10]. To calculate the transition rates for the transitions from the sublevels of the $^4F_{3/2}$ manifold to those lower manifolds at room temperature, the Boltzmann distribution factor $\exp(-\Delta E/kT)$ describing the distribution of the population density among all of the sublevels of $^4F_{3/2}$ should be considered. These factors for two sublevels of $^4F_{3/2}$ are 0.5585 and 0.4415 at 300 K respectively. The relation between the transition rate and line-strength of the fluorescence is as follows:

$$A(\alpha J, \alpha' J') = [64\pi^4 f^3 e^2/3h(2J+1)]N S_{JJ'} \tag{10}$$

$$S_{JJ'} = (1/e^2)\sum_{i,f}|\langle\Psi_{Ji}|P_{\xi\beta}|\Psi_{J'f}\rangle|^2 \tag{11}$$

where $N = (N_\pi + 2N_\sigma)/3$, $N_{\sigma,\pi} = n_{\sigma,\pi}(n^2_{\sigma,\pi}+2)^2/9$. The Sellmeier equations of $n_{\sigma,\pi}$ are given in [21], and the experimental transition rates from $^4F_{3/2}$ are given by Jaque *et al* [2] and listed in table 6.

Table 6. Spectroscopic experimental results for the NYAB crystal.

Transition from $^4F_{3/2}$	λ (nm)	n_π	n_σ	A (s^{-1}) (from [2])	A (s^{-1}) (present fit)
$^4F_{3/2} \rightarrow {}^4 I_{9/2}$	886	1.6924	1.7642	1637	1616
$^4F_{3/2} \rightarrow {}^4 I_{11/2}$	1067	1.6904	1.7616	1430	1412
$^4F_{3/2} \rightarrow {}^4 I_{13/2}$	1348	1.6887	1.7595	235	269

The fit to the experimental transition rates finally gives the odd CF parameters as follows:

$$C_{\tilde{1}}^3 = 538\mathrm{i} \qquad C_{\tilde{1}}^5 = -464\mathrm{i}. \tag{12}$$

Conversely,

$$B_{33} = -380\mathrm{i} \qquad B_{53} = -328\mathrm{i}. \tag{13}$$

Note that a constraint ratio $B_{53}/B_{33} = 0.64$ calculated by point-charge model is put in the fit so as to rule out the other minima and to find reasonable odd CF parameters in accordance with the physical reality. As shown in table 6, the calculated transition rates agree well with the experimental values. By (9) and (12), the radiative rates and the polarizations for the transition from sublevels of $^4F_{3/2}$ to those of $^4I_{9/2}$, $^4I_{11/2}$, $^4I_{13/2}$ can be estimated respectively, and the results are listed in tables 7 and 8.

Table 7. The calculated transition rates of $^4F_{3/2} \rightarrow {}^4 I_{9/2}$ in NYAB at 300 K.

Transition	λ	A_{ij} (s^{-1})	
$^4F_{3/2} \rightarrow {}^4 I_{9/2}$	(nm)	π	σ
a → a	877	116	179
→ b	881	—	392
→ c	887	114	285
→ d	891	—	170
→ e	901	133	163
b → a	873	—	2
→ b	877	46	—
→ c	883	—	∼0
→ d	887	14	—
→ e	897	—	2

To determine the fluorescence spectrum from $^4F_{3/2}$, one requires to know the shape of the spectral line. At very low temperature, the width of a spectral line is dominated by the crystal defect's inhomogeneous broadening, which is independent of the temperature. So the line shape is usually Gaussian. For a crystal such as NYAB at temperature (T) above 150 K, the homogeneous broadening caused by Raman phonon scattering, which is proportional to T^7, will dominate over the inhomogeneous broadening, and the line shape is normally Lorentzian [22].

The emission cross section σ for a spectral line can be expressed as:

$$\sigma = \sigma_0 \frac{(\Delta\nu/2)^2}{(\nu_0 - \nu)^2 + (\Delta\nu/2)^2} \tag{14}$$

Table 8. The calculated transition rates of $^4F_{3/2} \rightarrow {}^4 I_{11/2}$ in NYAB at 300 K.

Transition $^4F_{3/2} \rightarrow {}^4 I_{11/2}$	λ (nm)	A_{ij} (s^{-1}) π	σ
a → a	1060	41	29
→ b	1062	—	349
→ c	1064	127	7
→ d	1073	93	∼0
→ e	1079	—	253
→ f	1084	103	32
b → a	1054	—	52
→ b	1056	49	—
→ c	1058	—	92
→ d	1068	—	96
→ e	1073	68	—
→ f	1076	—	20

where ν_0 is the peak frequency of the transition; $\Delta\nu$ is the full width at half-maximum (FWHM); σ_0 is the peak cross section. For a Lorentzian line shape ($i \rightarrow j$)

$$\sigma_0 = \frac{\lambda_{ij}^2 A_{ij}}{4\pi^2 n^2 \Delta\nu}. \tag{15}$$

Based on Jaque's fluorescence polarized spectra at room temperature (see figures 1 and 2), $\Delta\nu$ of the transitions $^4F_{3/2} \rightarrow {}^4 I_{9/2}$ and $^4F_{3/2} \rightarrow {}^4 I_{11/2}$, $^4I_{13/2}$ can be estimated as about 6.445×10^{11} Hz and 4.50×10^{11} Hz respectively.

Figure 1 shows the polarized emission spectra in the infrared spectral domain obtained under excitation at 750 nm at room temperature [2]. Three peak groups correspond to the transition $^4F_{3/2} \rightarrow {}^4 I_{9/2}$, $^4I_{11/2}$ and $^4I_{13/2}$ respectively. Figure 2 shows the stimulated emission cross section as a function of the wavelength experimentally determined from the $^4F_{3/2} \rightarrow {}^4 I_{11/2}$ emission spectrum. The calculated emission spectra in this study are shown in figures 3–5. Now let us compare the calculated spectra with the experiment. Figure 3 agrees with figure 1 on the whole. The position and intensity of five main peaks appearing in the σ-polarization for the transition $^4F_{3/2} \rightarrow {}^4 I_{9/2}$ agree well with the experiment. In figure 4, the strongest peak in σ-spectra for $^4F_{3/2} \rightarrow {}^4 I_{11/2}$ shows at 1062 nm with a emission cross section of approximately 7.8×10^{-20} cm^2, which is close to the experimental value reported by Jaque ($\sigma = 1 \times 10^{-19}$ cm^2 at $\lambda = 1062.6$ nm in σ-spectra) [2]. In figure 5, the strongest peak in σ-spectra for $^4F_{3/2} \rightarrow {}^4 I_{9/2}$ appears at 881 nm with a cross section of about 4.1×10^{-20} cm^2, which corresponds to the reality in figure 1. However, the calculated results are not in complete agreement with the experiment. As shown in figures 3 and 4, the calculated cross sections of π-spectra for $^4F_{3/2} \rightarrow {}^4 I_{11/2}$ are much less than the experimental values. The positions and intensities of some peaks in figure 4 also disagree with those in figure 2. The reason for these inconsistencies may be the fact that we have not included the effect of the seventh-order odd CF components while these components may play an important role for the π-polarization transition. Taking into account the role of the seventh-order CF Hamiltonian, the agreement between the calculated and experimental spectra can be further improved, and this study is under way. In our calculation, we assume that the CF splitting is independent of the temperature. In fact, energy levels at 300 K are different from those at 10 K, which is maybe the reason that leads to the shift of the central wavelength of the peak.

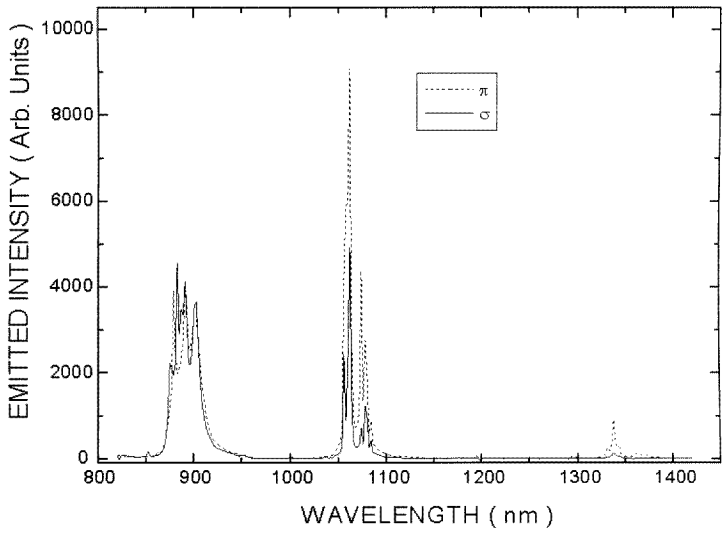

Figure 1. The polarized emission spectra in the infrared spectral domain obtained under excitation at 750 nm at room temperature for NYAB.

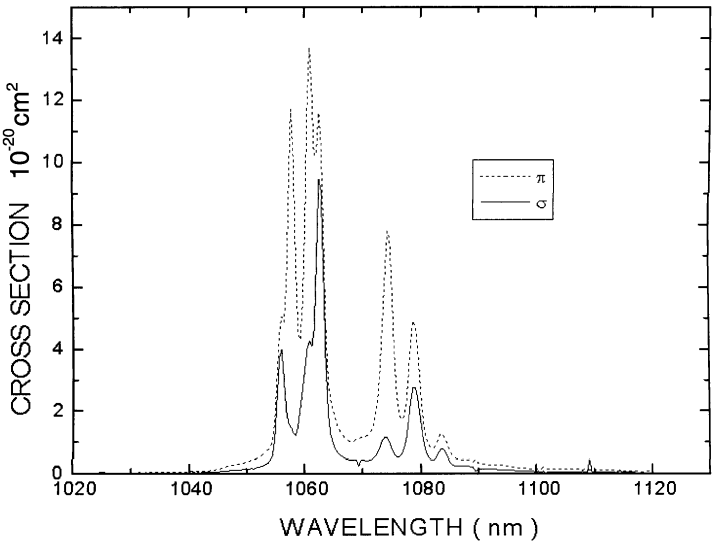

Figure 2. The stimulated emission cross section as a function of the wavelength experimentally determined from the $^4F_{3/2} \rightarrow {}^4 I_{11/2}$ emission spectrum.

Once the odd CF parameters are determined, we can calculate three JO intensity parameters Ω_λ ($\lambda = 2, 4, 6$) by the following expression [23]:

$$\Omega_\lambda = (2\lambda + 1) \sum_{k\mu} \frac{|C_\mu^k|^2}{(2k+1)\Delta^2(n'l')} \times \left[2\langle nl|r|n'l'\rangle \langle nl\|C^{(1)}\|n'l'\rangle \langle n'l'\|C^{(k)}\|nl\rangle \begin{Bmatrix} 1 & k & \lambda \\ l & l & l' \end{Bmatrix} \right]^2. \tag{16}$$

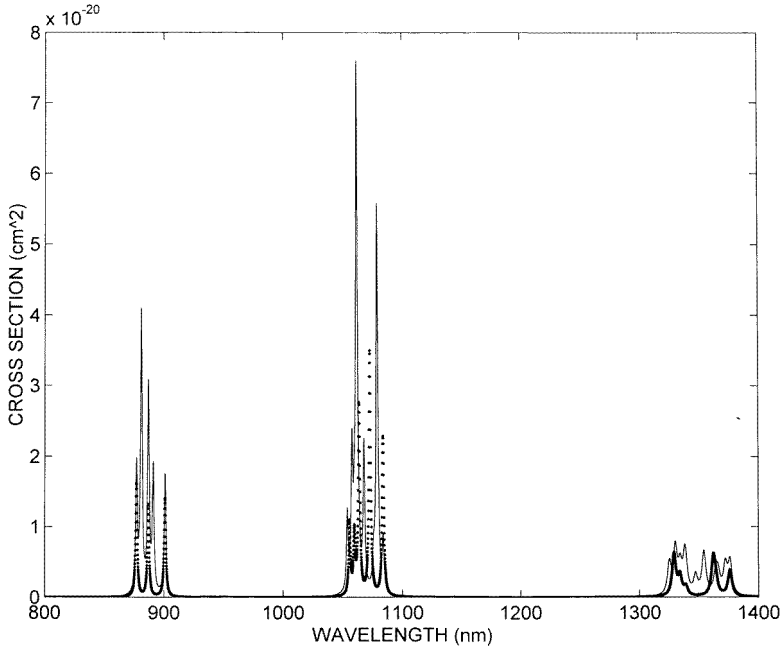

Figure 3. The calculated emission spectra for the transitions ($^4F_{3/2} \rightarrow {}^4 I_{9/2}$, $^4I_{11/2}$ and $^4I_{13/2}$) at 300 K for NYAB. The solid lines show σ-spectra and those with the dotted lines show π-spectra.

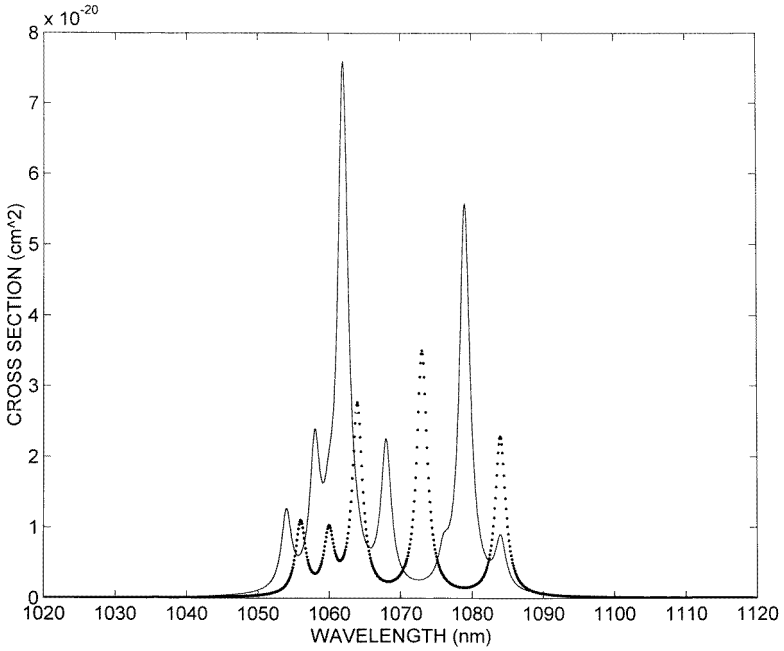

Figure 4. The calculated emission cross section as a function of the wavelength for the transition $^4F_{3/2} \rightarrow {}^4 I_{11/2}$ at 300 K for NYAB. The solid lines show σ-spectra and those with the dotted lines show π-spectra.

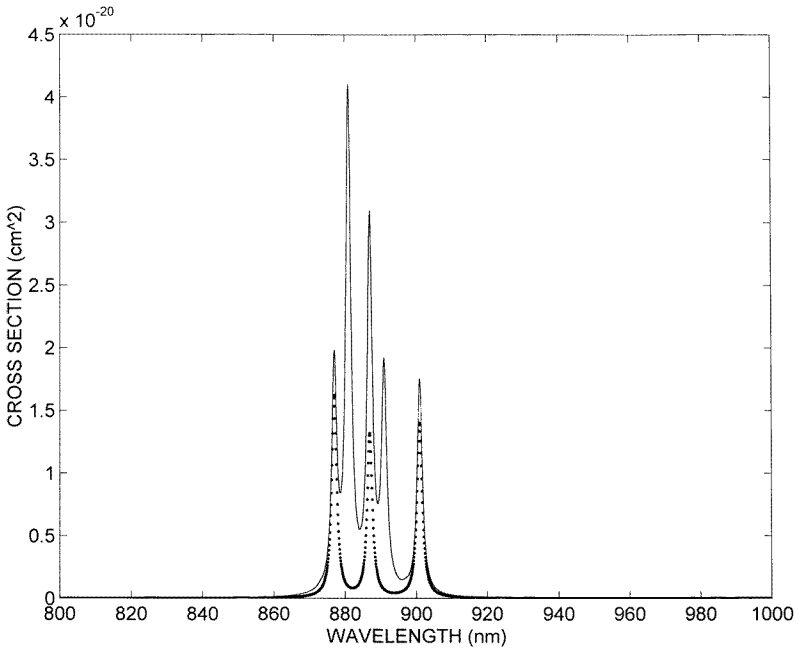

Figure 5. The calculated emission cross section as a function of the wavelength for the transition $^4F_{3/2} \rightarrow ^4 I_{9/2}$ at 300 K for NYAB. The solid lines show σ-spectra and those with the dotted lines show π-spectra.

Finally, we obtain: $\Omega_2 = 0.68 \times 10^{-20}$, $\Omega_4 = 4.72 \times 10^{-20}$, $\Omega_6 = 3.77 \times 10^{-20}$ (units: cm^2). The calculated Ω_4 and Ω_6 are in agreement with the experimental values ($\Omega_4 = 5.04 \times 10^{-20}$, $\Omega_6 = 3.11 \times 10^{-20}$) obtained from the absorption spectra [2], which confirms that the calculation method for the line-to-line transitions is reliable and useful. This method can also be used to predict the JO intensity parameters of other crystals.

5. Conclusion

A group-chain ($SO_3 \supset O \supset D_3$) scheme analysis has been carried out for Nd^{3+} ions of $YAl_3(BO_3)_4$ in D_3 symmetry sites. With the aid of the least-squares fit programs, the CF level fitting of the states $^4I_{9/2}$, $^4I_{11/2}$, $^4I_{13/2}$ and $^4F_{3/2}$ (20 levels) is performed. The even CF parameters and the wavefunctions of Stark sublevels have been obtained. The RMS of the fit is 8.95 cm^{-1} and the group attributes of the Stark levels compare well with the experiment on the whole, which indicates the success of the CF level fitting.

On the basis of wavefunctions obtained, the g-factors of the ground and excited manifolds ($^4I_{9/2}$, $^4I_{11/2}$, $^4I_{13/2}$ and $^4F_{3/2}$) are calculated, which confirms the partial g-sums rule of Karayianis. The g-factors of the ground level of $^4I_{9/2}$ are predicted to be $g_\parallel = 1.332$ and $g_\perp = 3.552$, as may be confirmed by the future experiment.

Neglecting the effect of the seventh-order CF interactions, the ED transition matrix element can be derived in view of the group-chain $SO_3 \supset O \supset D_3 \supset C_3$ in NYAB. By the fit to the experimental transition rates for the transitions $^4F_{3/2} \rightarrow ^4 I_{9/2}$, $^4I_{11/2}$ and $^4I_{13/2}$, the odd CF parameters can be obtained: $C_{\bar{1}}^3 = 538i$, $C_{\bar{1}}^5 = -464i$. The line-to-line transition rates from $^4F_{3/2}$ are subsequently given. Theoretically calculated emission spectra

at room temperature basically agree with the experiment. Once the odd CF parameters are determined, the JO intensity parameters can be theoretically calculated. The values of the calculated Ω_4 and Ω_6 compare well to the experiment.

In general, CF analysis by using the group-chain scheme has been effectively applied to Nd^{3+} ions in $YAl_3(BO_3)_4$. Some of our results may be used as a guide to the development of the NYAB laser.

Wavefunctions for the crystal-field energy levels in NYAB ($SO_3 \supset O \supset D_3$)

$^4I_{9/2}$ (a) $0.2306\left|\frac{9}{2}\frac{1}{2}\frac{1}{2}\right\rangle + 0.8347\left|\frac{9}{2}\frac{3}{2_0}\frac{1}{2}\right\rangle - 0.5001\left|\frac{9}{2}\frac{3}{2_1}\frac{1}{2}\right\rangle$ (Γ_4)

(b) $0.8315\left|\frac{9}{2}\frac{3}{2_0}\pm\frac{3}{2}\right\rangle + (-0.5348 \pm 0.1504\mathrm{i})\left|\frac{9}{2}\frac{3}{2_1}\pm\frac{3}{2}\right\rangle$ ($\Gamma_{5,6}$)

(c) $0.2011\left|\frac{9}{2}\frac{1}{2}\frac{1}{2}\right\rangle + 0.4619\left|\frac{9}{2}\frac{3}{2_0}\frac{1}{2}\right\rangle + 0.8638\left|\frac{9}{2}\frac{3}{2_1}\frac{1}{2}\right\rangle$ (Γ_4)

(d) $(0.5348 \pm 0.1504\mathrm{i})\left|\frac{9}{2}\frac{3}{2_0}\pm\frac{2}{2}\right\rangle + 0.8315\left|\frac{9}{2}\frac{3}{2_1}\pm\frac{3}{2}\right\rangle$ ($\Gamma_{5,6}$)

(e) $0.9520\left|\frac{9}{2}\frac{1}{2}\frac{1}{2}\right\rangle - 0.2998\left|\frac{9}{2}\frac{3}{2_0}\frac{1}{2}\right\rangle - 0.0614\left|\frac{9}{2}\frac{3}{2_1}\frac{1}{2}\right\rangle$ (Γ_4)

$^4I_{11/2}$ (a) $-0.9841\left|\frac{11}{2}\frac{1}{2}\frac{1}{2}\right\rangle - 0.0666\left|\frac{11}{2}\frac{3}{2_0}\frac{1}{2}\right\rangle - 0.1590\left|\frac{11}{2}\frac{3}{2_1}\frac{1}{2}\right\rangle + 0.0419\left|\frac{11}{2}\frac{\tilde{1}}{2}\frac{1}{2}\right\rangle$ (Γ_4)

(b) $0.9054\left|\frac{11}{2}\frac{3}{2_0}\pm\frac{3}{2}\right\rangle + (0.3594 \mp 0.2260\mathrm{i})\left|\frac{11}{2}\frac{3}{2_1}\pm\frac{3}{2}\right\rangle$ ($\Gamma_{5,6}$)

(c) $-0.0535\left|\frac{11}{2}\frac{1}{2}\frac{1}{2}\right\rangle + 0.9924\left|\frac{11}{2}\frac{3}{2_0}\frac{1}{2}\right\rangle - 0.0596\left|\frac{11}{2}\frac{3}{2_1}\frac{1}{2}\right\rangle + 0.0937\left|\frac{11}{2}\frac{\tilde{1}}{2}\frac{1}{2}\right\rangle$ (Γ_4)

(d) $0.0703\left|\frac{11}{2}\frac{1}{2}\frac{1}{2}\right\rangle - 0.0972\left|\frac{11}{2}\frac{3}{2_0}\frac{1}{2}\right\rangle - 0.1351\left|\frac{11}{2}\frac{3}{2_1}\frac{1}{2}\right\rangle + 0.9835\left|\frac{11}{2}\frac{\tilde{1}}{2}\frac{1}{2}\right\rangle$ (Γ_4)

(e) $(-0.3594 \mp 0.2260\mathrm{i})\left|\frac{11}{2}\frac{3}{2_0}\pm\frac{3}{2}\right\rangle + 0.9054\left|\frac{11}{2}\frac{3}{2_1}\pm\frac{3}{2}\right\rangle$ ($\Gamma_{5,6}$)

(f) $-0.1538\left|\frac{11}{2}\frac{1}{2}\frac{1}{2}\right\rangle + 0.0363\left|\frac{11}{2}\frac{3}{2_0}\frac{1}{2}\right\rangle + 0.9762\left|\frac{11}{2}\frac{3}{2_1}\frac{1}{2}\right\rangle + 0.1487\left|\frac{11}{2}\frac{\tilde{1}}{2}\frac{1}{2}\right\rangle$ (Γ_4)

$^4I_{13/2}$ (a) $0.9565\left|\frac{13}{2}\frac{1}{2}\frac{1}{2}\right\rangle - 0.1146\left|\frac{13}{2}\frac{3}{2_0}\frac{1}{2}\right\rangle + 0.1429\left|\frac{13}{2}\frac{3}{2_1}\frac{1}{2}\right\rangle + 0.0469\left|\frac{13}{2}\frac{\tilde{1}}{2_0}\frac{1}{2}\right\rangle$
$+0.2222\left|\frac{13}{2}\frac{\tilde{1}}{2_1}\frac{1}{2}\right\rangle$ (Γ_4)

(b) $(-0.5946 \pm 0.3599\mathrm{i})\left|\frac{13}{2}\frac{3}{2_0}\pm\frac{3}{2}\right\rangle + 0.7189\left|\frac{13}{2}\frac{3}{2_1}\pm\frac{1}{2}\right\rangle$ ($\Gamma_{5,6}$)

(c) $-0.2441\left|\frac{13}{2}\frac{1}{2}\frac{1}{2}\right\rangle - 0.4480\left|\frac{13}{2}\frac{3}{2_0}\frac{1}{2}\right\rangle + 0.7682\left|\frac{13}{2}\frac{3}{2_1}\frac{1}{2}\right\rangle - 0.1491\left|\frac{13}{2}\frac{\tilde{1}}{2_0}\frac{1}{2}\right\rangle$
$+0.3570\left|\frac{13}{2}\frac{\tilde{1}}{2_1}\frac{1}{2}\right\rangle$ (Γ_4)

(d) $-0.0387\left|\frac{13}{2}\frac{1}{2}\frac{1}{2}\right\rangle + 0.4524\left|\frac{13}{2}\frac{3}{2_0}\frac{1}{2}\right\rangle - 0.1598\left|\frac{13}{2}\frac{3}{2_1}\frac{1}{2}\right\rangle - 0.6082\left|\frac{13}{2}\frac{\tilde{1}}{2_0}\frac{1}{2}\right\rangle$
$+0.6312\left|\frac{13}{2}\frac{\tilde{1}}{2_1}\frac{1}{2}\right\rangle$ (Γ_4)

(e) $-0.1114\left|\frac{13}{2}\,\frac{1}{2}\,\frac{1}{2}\right\rangle+0.4427\left|\frac{13}{2}\,\frac{3}{2_0}\,\frac{1}{2}\right\rangle+0.1630\left|\frac{13}{2}\,\frac{3}{2_1}\,\frac{1}{2}\right\rangle+0.7539\left|\frac{13}{2}\,\frac{\tilde{1}}{2_0}\,\frac{1}{2}\right\rangle$
$+0.4435\left|\frac{13}{2}\,\frac{\tilde{1}}{2_1}\,\frac{1}{2}\right\rangle$ (Γ_4)

(f) $0.7189\left|\frac{13}{2}\,\frac{3}{2_0}\pm\frac{3}{2}\right\rangle+(0.5946\pm 0.3599\mathrm{i})\left|\frac{13}{2}\,\frac{3}{2_1}\pm\frac{3}{2}\right\rangle$ $(\Gamma_{5,6})$

(g) $-0.1080\left|\frac{13}{2}\,\frac{1}{2}\,\frac{1}{2}\right\rangle-0.6209\left|\frac{13}{2}\,\frac{3}{2_0}\,\frac{1}{2}\right\rangle-0.5808\left|\frac{13}{2}\,\frac{3}{2_1}\,\frac{1}{2}\right\rangle+0.1933\left|\frac{13}{2}\,\frac{\tilde{1}}{2_0}\,\frac{1}{2}\right\rangle$
$+0.4776\left|\frac{13}{2}\,\frac{\tilde{1}}{2_1}\,\frac{1}{2}\right\rangle$ (Γ_4)

$^4\mathrm{F}_{3/2}$ (a) $\left|\frac{3}{2}\,\frac{3}{2}\,\frac{1}{2}\right\rangle$ (Γ_4)

(b) $\left|\frac{3}{2}\,\frac{3}{2}\pm\frac{3}{2}\right\rangle$. $(\Gamma_{5,6})$.

References

[1] Luo Zundu, Jiang Aidong, Huang Yichuan and Qiu Minwang 1989 *Chin. Phys. Lett.* **6** 440
[2] Jaque D, Capmany J, Luo Z D and Solé J G 1997 *J. Phys.: Condens. Matter* **9** 9715
[3] Lu B, Wang J, Pan H, Jiang M, Liu E and Hou X 1989 *J. Appl. Phys.* **66** 6052
[4] Amano S and Mochizuki T 1991 *Nonlin. Opt.* **1** 297
[5] Zhao T, Luo Z, Huang Y, Qiu M and Chen G 1994 *Opt. Comm.* **109** 115
[6] Hemmati H 1992 *IEEE J. Quantum Electron.* **QE-28** 1169
[7] Li Z, Fan Q, Zhou F, Ma J and Xue Q 1994 *Opt. Eng.* **33** 1138
[8] Jaque D, Capmany J, Luo Z D, Jiang A and Solé J G *J. Opt. Soc. Am.* B submitted
[9] Luo Zundu and Huang Yidong 1993 *J. Phys.: Condens. Matter* **5** 6949
[10] Luo Zundu and Huang Yidong 1994 *J. Phys.: Condens. Matter* **6** 3737
[11] Chen Xueyuan and Luo Zundu 1996 *J. Phys.: Condens. Matter* **8** 2571
[12] Chen Xueyuan and Luo Zundu 1997 *J. Phys.: Condens. Matter* **9** 4197
[13] Chen Xueyuan and Luo Zundu 1997 *J. Phys.: Condens. Matter* **9** 7981
[14] Butler P H 1981 *Point Group Symmetry Application: Method and Tables* (New York: Plenum)
[15] Judd B R 1962 *Phys. Rev.* **127** 750
[16] Ofelt G S 1962 *J. Chem. Phys.* **37** 511
[17] Sachs M 1963 *Solid State Theory* (New York: McGraw-Hill)
[18] Wybourne B G 1961 *J. Chem. Phys.* **34** 279
[19] Morrison C A and Leavitt R P 1979 *J. Chem. Phys.* **71** 2366
[20] Karayianis N 1971 *J. Chem. Phys.* **55** 3734
[21] Luo Z D, Lin J T, Jiang A D, Huang Y C and Qiu M W 1989 *Proc. SPIE* **1104** 132
[22] Kaminskii A A 1990 *Laser Crystals: their Physics and Properties* (London: Springer)
[23] Krupke W F 1966 *Phys. Rev.* **145** 325